UCLA
UCLA Previously Published Works

Title

Obtaining closure for a plane fin heat sink with elliptic scale-roughened surfaces for Volume Averaging Theory (VAT) based modeling

Permalink

https://escholarship.org/uc/item/4c20d1t9

Journal

International Journal of Thermal Sciences, 71

ISSN

12900729

Authors

Zhou, Feng
Catton, Ivan

Publication Date

2013-09-01

DOI

10.1016/j.ijthermalsci.2013.04.020

Peer reviewed

CrossMark

Obtaining closure for a plane fin heat sink with elliptic scale-roughened surfaces for Volume Averaging Theory (VAT) based modeling

Feng Zhou*, Ivan Catton

Department of Mechanical and Aerospace Engineering, University of California, 48-121 Engineering IV, 420 Westwood Plaza, Los Angeles, CA 90095, USA

ABSTRACT

Closure for a Volume Averaging Theory (VAT) based model of a plane fin heat sink (PFHS) with elliptic scale-roughened surfaces is obtained by evaluating the closure terms for the model using Computer Fluid Dynamics (CFD) code. Modeling a PFHS as porous media based on VAT, specific geometry can be accounted for in such a way that the details of the original structure can be replaced by their averaged counterparts and the VAT based governing equations can be efficiently solved for a wide range of parameters. To complete the VAT based model, proper closure is needed, which is related to a local friction factor and a heat transfer coefficient of a Representative Elementary Volume (REV). The terms in the closure expressions are complex and sometimes relating experimental data to the closure terms is difficult. In this work we use CFD to obtain detailed solutions of flow and heat transfer through an element of the elliptic scale-roughened heat sink and use these results to evaluate the closure terms needed for a fast running VAT based code, which can then be used to solve the heat transfer characteristics of a higher level heat sink. The objective is to show how CFD can be used in place of a detailed, often formidable, experimental effort to obtain closure for a VAT based model.

© 2013 Elsevier Masson SAS. All rights reserved.

1. Introduction

High heat fluxes in electronic chips are driving conflicting needs for elevated power dissipation requirement as well as reduced power consumption, size and weight, which makes thermal management an essential element in the development of these systems. A variety of techniques [1] for heat transfer enhancement have been developed, including ribs [2—6], pin fins [7—9], dimpled surfaces [10—12], surfaces with arrays of protrusions [13], and surface roughness. The design objective of these techniques is to significantly enhance convective heat transfer without substantially increasing in the streamwise pressure drop penalty.

Chang et al. [14—18] developed a new heat transfer enhancement technique using deepened circular scale-roughened surfaces. The surface scales are arranged in a staggered manner in-line on opposing walls. The authors compared $\overline{Nu}/Nu_\infty$ and $\overline{f}/f_\infty$ of the scale roughened surface with the flow and heat transfer results reported by different research groups for rib-roughened channels [2—6] and dimpled surfaces [10]. The heat transfer enhancement of the circular scale-roughened surface was surprisingly good and the

channel with forward flow presented a better thermal performance than the rib-roughened and dimpled surfaces. Correlations of Nusselt number and friction factor for circular scale-roughened channels were developed by Zhou et al. [19] to close their Volume Averaging Theory (VAT) based model for heat sink optimization purpose. Recently, six new types of elliptic scale-roughened surfaces are proposed by the present authors and compared with the original circular scale case [20]. Nusselt number ratios between the elliptic scale-roughened and smooth channel flows (Nu/Nu_∞) could be enhanced to be around 6.5, which is a 40% improvement compared to the circular scale-roughened channels. The geometrical details of the proposed elliptic scale-roughened surface are shown in Fig. 1(b) and (c).

Considering the thrilling heat transfer enhancement performance of the proposed elliptic scale-roughened surface, it could be applied to plane fin heat sinks to augment their heat dissipation capability, see Fig. 1(a), but further optimization is required. If one wants to optimize such a heat transfer device, simple equations are the only answer but they need to be made more rigorous and must include conjugate effects. In this work VAT, see Refs. [21—32], is used to develop the needed simple equations allowing clear rigorous statements to be made that define how the friction factor and heat transfer coefficient are to be determined. By modeling heat sinks as porous media, specific geometry can be accounted for

* Corresponding author.
  E-mail addresses: zhoufeng@ucla.edu, fengucla@gmail.com (F. Zhou).
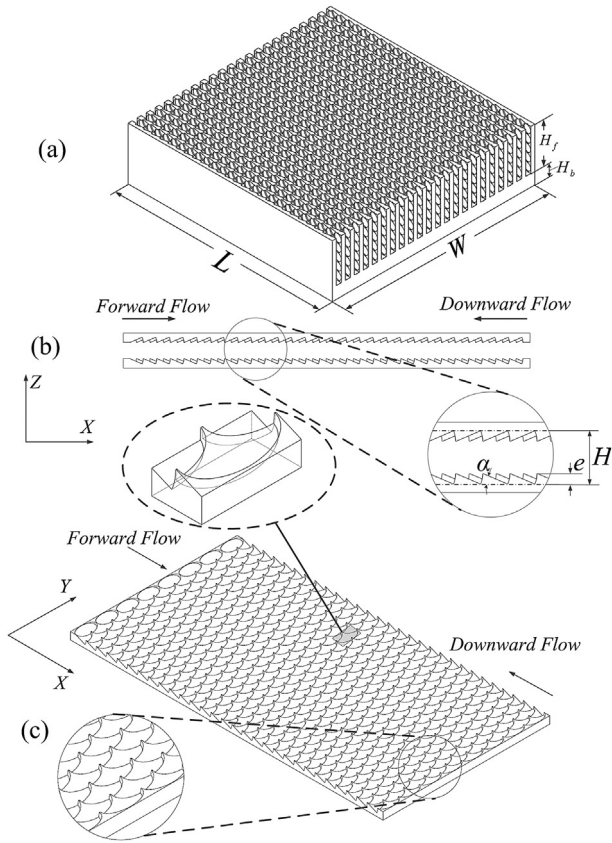
Fig. 1. Geometrical details of elliptic scale-roughened surface.

in such a way that the details of the original structure can be replaced by their averaged counterparts and the governing VAT equations can be solved for a wide range of design parameters. This 'porous media' model, which is a function only of porous media morphology, represented by porosity and specific surface area, and its closure, can easily be adapted to many different structures.

Closure theories for transport equations in heterogeneous media have been the primary measure of advancement and for measuring success in research on transport in porous media. Obtaining closure for the VAT based governing equation set is the most difficult aspect of using VAT to model and optimize a heat transfer device. The porosity and specific surface area are geometrically defined terms. The closure terms, which are related to a local friction factor and a heat transfer coefficient, can be obtained in two ways. The first is to rescale the available experimental data reported for fully developed flow, using the 'porous media' length scale suggested by VAT [24–26,28]. However, experimental methods are expensive and time consuming, as many different models must be fabricated and tested, and sometimes obtaining closure by relating experimental data to the closure terms is difficult. At this time, CFD is an alternative approach for evaluating these closure terms [19,33–38]. It should be noted that if CFD is used to obtain the closure, the friction factor and heat transfer will be calculated more rigorously by integrating the complete closure formula over the REV and validated using the available experimental data.

In the following presentation, an elliptic scale-roughened plane fin heat sink with forward flow is first modeled based on Volume Averaging Theory. 3-D numerical calculations are made to simulate the heat transfer and fluid flow across the channels and the CFD discretization is validated by comparison with the experimental data by Chang et al. [14]. Then, the rigorously derived closure terms

are evaluated over one of the selected REVs for a range of the design parameters, and correlations for friction factor and Nusselt number are developed for use with the simple equations.

2. VAT based modeling

A schematic diagram of a plate fin heat sink with scale-roughened surface is shown in Fig. 1(a). Generally, the air is forced to flow through the channels between the fins by a fan. The scales act to increase secondary flows and turbulence levels to enhance mixing, and form coherent fluid motions in the form of streamwise oriented vortices, and also to provide some heat transfer augmentation by increasing surface areas for convective heat transfer [1]. This is a problem of conjugate heat transfer within a heterogeneous hierarchical structure. It is not easy to optimize this kind of problem since many parameters are required to describe the geometry. Simple equations are the only answer if one wants to find the optimum configuration for these kinds of conjugate heat transfer devices.

2.1. VAT based governing equations

Based on rigorous averaging techniques developed by Whitaker [23,24] who focused on solving linear diffusion problems and by Travkin and Catton [26,28] who focused on solving nonlinear turbulent diffusion problems, the thermal physics and fluid mechanics governing equations in heterogeneous porous media were developed from the Navier–Stokes equation and the thermal energy equations. This is the starting point for studying flow and heat transfer in porous media and also the basis of the present work. For more details of modeling of flow and heat transfer through porous media and how Volume Averaging Theory was developed, refer to Refs. [39–41].

In this section, a model based on VAT is developed to describe transport phenomena in plane fin heat sinks with shielded top, at which a boundary condition of nonslip wall is applied. The air flow is considered to be 'porous flow', in which the term 'porous' is used in a broad sense.

The momentum equation is

$$0 = -\frac{1}{\rho_\mathrm{f}} \frac{\mathrm{d}\langle \overline{p} \rangle_\mathrm{f}}{\mathrm{d}x} + f^* \frac{S_\mathrm{w}}{\langle m(z) \rangle} \frac{\tilde{\overline{u}}^2}{2} + \frac{\partial}{\partial z}\left(\langle m(z) \rangle (\nu + \tilde{\nu}_\mathrm{t}) \, \frac{\partial \tilde{\overline{u}}}{\partial z} \right) \quad (1)$$

The energy equation for fluid phase is

$$\rho_\mathrm{f} c_\mathrm{pf} \langle m \rangle \tilde{\overline{u}} \frac{\partial \tilde{\overline{T}}_\mathrm{f}}{\partial x} = \frac{\partial}{\partial z}\left(\langle m \rangle \left(k_\mathrm{f} + \tilde{k}_\mathrm{t} \right) \frac{\partial \tilde{\overline{T}}_\mathrm{f}}{\partial z} \right) + h^* S_\mathrm{w}\left(\tilde{T}_\mathrm{s} - \tilde{\overline{T}}_\mathrm{f} \right) \quad (2)$$

The energy equation for solid phase is

$$\frac{\partial}{\partial x}\left[(1 - \langle m \rangle) k_\mathrm{s} \frac{\partial \tilde{T}_\mathrm{s}}{\partial x} \right] + \frac{\partial}{\partial z}\left[(1 - \langle m \rangle) k_\mathrm{s} \frac{\partial \tilde{T}_\mathrm{s}}{\partial z} \right] = h^* S_\mathrm{w}\left(\tilde{T}_\mathrm{s} - \tilde{\overline{T}}_\mathrm{f} \right) \quad (3)$$

2.2. Closure terms of the VAT equations

To complete the VAT based model, four closure terms need to be evaluated. It is believed that the only way to achieve substantial gains is to maintain the connection between porous media morphology and the rigorous formulation of mathematical equations for transport.
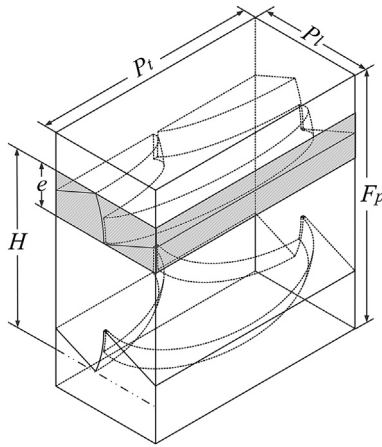
Fig. 2. Representative Elementary Volume (REV) for a PFHS with elliptic scale-roughened surfaces.

Two of the closure terms, the averaged porosity and the specific surface area are geometrically defined and it is quite easy to determine them if one selects the REV correctly. The selection for a PFHS with elliptic scale roughened surface, see Fig. 2, is seen to repeat in both the cross-stream and flow directions. Therefore, the porosity is

$$\langle m \rangle = 1 - \frac{\Delta \Omega_s}{\Delta \Omega} = \frac{H - 2\kappa e}{F_p} \tag{4}$$

in which, $\Delta \Omega$ is the volume of the REV defined as

$$\Delta \Omega = P_t P_l F_p \tag{5}$$

$\Delta \Omega_s$ is the volume of the solid part of the REV defined by

$$\Delta \Omega_s = P_t P_l (F_p - H) + 2\kappa e P_t P_l \tag{6}$$

in which κ is the ratio of the solid volume of the scale to the total volume of the $e \times P_t \times P_l$ slab, see the shaded part in Fig. 2. It can easily be shown that κ is a constant and $\kappa = 3/4 - \pi/8$.

The specific surface area, S_w, is defined as

$$S_w = \frac{A_w}{\Delta \Omega} = \frac{2P_t P_l + \pi \left[\frac{3}{4}(P_t + P_l) - \frac{1}{2}\sqrt{P_t P_l} \right] e}{P_t P_l F_p} \tag{7}$$

At this point, the VAT based model of elliptic scale-roughened PFHS is still not fully closed. The other two closure terms are the
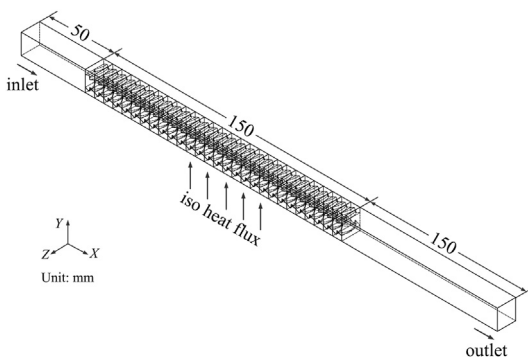

Fig. 3. Computational domain. The length of the extended regions was not drawn in scale.

local friction factor, f^*, in the momentum equation and the local heat transfer coefficient, h^*, in the VAT energy equations and remain to be evaluated. To evaluate the closure terms, a commercial Finite Volume Method (FVM)-based code, CFX, was used to analyze the convective heat transfer in three-dimensional channels with opposing elliptic scale-roughened walls.

3. Numerical method and procedures

3.1. Computational domain and boundary conditions

The local closure values or closure values for fully developed flow and heat transfer are the only kinds of closure values that have physical meaning when describing transport phenomena with VAT based equations. For this reason, attention should be paid to the selection of physical model. The computational domain should be long enough, so that closure can be evaluated over an REV that is not affected by entrance or re-circulation effects near the outlet [42]. A computational domain was selected as Fig. 3 shows.

The air velocity profile at the entrance is not uniform because of the fin thickness. The computational domain is extended upstream a distance of one third of the stream-wise channel length so that a uniform velocity distribution can be ensured at the domain inlet. The computational domain is extended downstream a stream-wise channel length, so that at the outer flow boundary no flow re-circulation exits. The boundary conditions applied to the computational domain are tabulated in Table 1.

3.2. Grid system

The grid systems for all the scale-roughened channel models are built by Ansys Meshing. Due to the roughness of the wall, an unstructured tetra-mesh is created for the scale-roughened test channel, with prism layers being inserted in the near wall region. In the extended regions, a coarser and structured hex-mesh is adopted to conserve computational resources. A grid system with a gradual variation in and after the scale-roughened test channel is used to avoid the undesirable effect of an abrupt grid width change in the computing region. The grid system for one of the models is shown in Fig. 4.

Grid independence tests were made carefully by recursive refinement and comparison between the numerical simulation results. The above process was repeated until the variation of Nusselt number and friction factor was less than 0.5%, so that the numerical predictions can be regarded as grid-independent. With the turbulence predictions employed, the meshes near the fluid solid interface are fine enough to resolve the flow behavior close to the no-slip wall. For all the simulation cases, y^+ values in the near-wall region are less than 1.

3.3. Mathematical model

The air flow is assumed to be three-dimensional, incompressible, steady state. In the low Reynolds number region, the flow is assumed to be laminar, while for $Re > 2000$, a turbulent model is

Table 1
Boundary conditions.

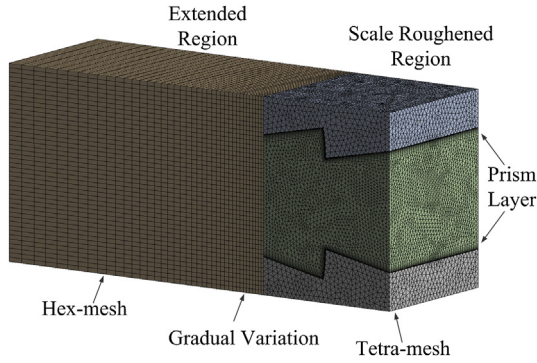| Inlet	$u = \text{const}, v = w = 0, T = \text{const}$
Outlet	$\frac{\partial u_i}{\partial x} = \frac{\partial T}{\partial x} = 0$
Eight surfaces of the extended region	Symmetric, slip and adiabatic wall
Interface between air and solid	No-slip, no thermal resistance
The bottom of the scale roughened wall	Iso heat flux
The other surfaces	Symmetric

Fig. 4. Example of the grid system. Only part of the whole model is shown.

adopted. Buoyancy and radiation heat transfer effects are not taken into consideration.

The CFX solver solves the discrete system of linearized equations using a multi-grid accelerated Incomplete Lower Upper (ILU) factorization technique and rapidly removes local errors in the solution. The algebraic multi-grid scheme is used to accelerate the convergence of the solver by computing the corrections on a series of coarse grid levels. The CFD code solves the Reynolds-averaged Navier–Stokes equations with a high resolution scheme for the advection terms as well as turbulence numerics. The fully coupled momentum and energy equations are solved simultaneously. In all simulations, the second-order upwind scheme is used for the discretization of the momentum and energy equations. The RMS type residual for solution convergence criteria is set to be 10^{-5} for the momentum balance and 10^{-6} for the energy equation. The three-dimensional governing equations for continuity, momentum and energy are as follows:

(1) Continuity equation

$$\frac{\partial \rho u_i}{\partial x_i} = 0 \tag{8}$$

(2) Momentum equation

$$\rho u_j \frac{\partial u_i}{\partial x_j} = \frac{\partial}{\partial x_j}\left[(\mu + \mu_t)\frac{\partial u_i}{\partial x_j}\right] - \frac{\partial p}{\partial x_i} \tag{9}$$

(3) Energy equation

$$\rho u_j \frac{\partial T}{\partial x_j} = \frac{\partial}{\partial x_j}\left[\left(\frac{\mu}{Pr} + \frac{\mu_t}{Pr_t}\right)\frac{\partial T}{\partial x_j}\right] \tag{10}$$

The k–ω based Shear–Stress-Transport (SST) model with automatic wall function treatment is used to predict the turbulent flow and heat transfer through the channel. The SST model blends the robust and accurate formulation of the k–ω model in the near-wall region with the free-stream independence of the k–ε model in the far field. The SST model gives a highly accurate prediction of the onset and the amount of flow separation under adverse pressure gradients by the inclusion of transport effects into the formulation of the eddy-viscosity. This results in a major improvement in terms of flow separation predictions. The superior performance of the SST model has been demonstrated for high accuracy boundary layer simulations in a large number of validation studies.

Menter [43,44] proposed the equations for the SST model as

$$\frac{D(\rho k)}{Dt} = \tilde{P}_k - \beta^* \rho k \omega + \frac{\partial}{\partial x_j}\left[(\mu + \sigma_k \mu_t)\frac{\partial k}{\partial x_i}\right] \tag{11}$$

$$\frac{D(\rho \omega)}{Dt} = \alpha \rho S^2 - \beta \rho \omega^2 + \frac{\partial}{\partial x_i}\left[(\mu + \sigma_\omega \mu_t)\frac{\partial \omega}{\partial x_i}\right]$$
$$+ 2(1 - F_1)\rho \sigma_{\omega 2}\frac{1}{\omega}\frac{\partial k}{\partial x_i}\frac{\partial \omega}{\partial x_i} \tag{12}$$

where the blending function F_1 is defined by:

$$F_1 = \tanh\left\{\left\{\min\left[\max\left(\frac{\sqrt{k}}{\beta^* \omega y}, \frac{500\nu}{y^2 \omega}\right), \frac{4\rho \sigma_{\omega 2} k}{CD_{k\omega} y^2}\right]\right\}^4\right\} \tag{13}$$

in which

$$CD_{k\omega} = \max\left(2\rho \sigma_{\omega 2}\frac{1}{\omega}\frac{\partial k}{\partial x_j}\frac{\partial \omega}{\partial x_j}, 10^{-10}\right) \tag{14}$$

The turbulent eddy viscosity is computed from:

$$\nu_t = \frac{a_1 k}{\max(a_1 \omega, SF_2)} \tag{15}$$

where S is the invariant measure of the strain rate and F_2 is a second blending function defined by

$$F_2 = \tanh\left\{\left[\max\left(2\frac{\sqrt{k}}{\beta^* \omega y}, \frac{500\nu}{y^2 \omega}\right)\right]^2\right\} \tag{16}$$

To prevent the build-up of turbulence in stagnation regions, a production limiter is used in the SST model:

$$P_k = \mu_t \frac{\partial u_i}{\partial x_j}\left(\frac{\partial u_i}{\partial x_j} + \frac{\partial u_j}{\partial x_i}\right) \rightarrow \tilde{P}_k = \min\left(P_k, 10 \cdot \beta^* \rho k \omega\right) \tag{17}$$

Each of the constants is a blend of the corresponding constants of the k–ε and the k–ω model:

$$\varphi = F_1 \varphi_1 + (1 - F_1)\varphi_2 \tag{18}$$

The constants for this model take the following values

$$\begin{aligned}
&\beta^* = 0.09, \\
&\alpha_1 = 5/9, \ \beta_1 = 3/40, \ \sigma_{k1} = 0.85, \ \sigma_{\omega 1} = 0.5, \\
&\alpha_2 = 0.44, \ \beta_2 = 0.0828, \ \sigma_{k2} = 1, \ \sigma_{\omega 2} = 0.856.
\end{aligned} \tag{19}$$

4. Closure evaluation

Closure evaluation described in this section consists of four parts. First, the two different length scales used to evaluate the flow and heat transfer characteristics of the elliptic scale-roughened channels are defined. Second, the computational model and the method adopted in current numerical simulations are verified and validated by comparing the CFD results with experimental data. Third, the mechanism of heat transfer enhancement by elliptic scales is analyzed. Fourth, two correlations which serve as closure for the VAT based model are developed based on the simulation results.

4.1. Length scales

Before evaluating the closure terms, it is interesting to note that using a particular length scale leads to a parameter that is very beneficial when evaluating the heat transfer coefficient and friction factor. It was shown by Travkin and Catton [28] that globular media morphologies can be described in terms of S_w, $\langle m \rangle$ and d_p and can generally be considered to be spherical particles with

$$S_w = \frac{6(1 - \langle m \rangle)}{d_p} \qquad (20)$$

$$D_h = \frac{2}{3} \frac{\langle m \rangle}{(1 - \langle m \rangle)} d_p \qquad (21)$$

This expression has the same dependency on equivalent pore diameter as found for a one diameter capillary morphology leading naturally to

$$S_w = \frac{6(1 - \langle m \rangle)}{d_p} = \frac{6(1 - \langle m \rangle)}{\frac{3}{2} \frac{(1 - \langle m \rangle)}{\langle m \rangle} D_h} = \frac{4\langle m \rangle}{D_h} \qquad (22)$$

This observation leads to defining a simple "universal" porous media length scale

$$D_h = \frac{4\langle m \rangle}{S_w} \qquad (23)$$

that meets the needs of both morphologies: capillary and globular. This was also recognized by Whitaker [24] when he used a very similar (differing by a constant) length scale to correlate heat transfer for a wide variety of morphologies. Zhou et al. [45] also showed that using the 'porous media' length scale is very beneficial in collapsing complex data yielding simple heat transfer and friction factor correlations. For the present scale-roughened channel, D_h is defined as

$$D_h = \frac{4\langle m \rangle}{S_w} = \frac{4 P_t P_l (H - 2\kappa e)}{2 P_t P_l + \pi \left[\frac{3}{4} (P_t + P_l) - \frac{1}{2} \sqrt{P_t P_l} \right] e} \qquad (24)$$

It can be seen that D_h is a function of e, P_t, P_l and H.

The Reynolds number defined using the VAT suggested length scale is

$$Re_{D_h} = \frac{\rho \tilde{\bar{u}} D_h}{\mu} \qquad (25)$$

To validate the CFD simulation results, the Reynolds number is defined the same as that used by Chang et al. [14]

$$Re = \frac{\rho u_m d_h}{\mu} \qquad (26)$$

in which d_h is the hydraulic diameter defined by

$$d_h = 2 \cdot H \cdot W / (H + W) \qquad (27)$$

The averaged Nusselt number in the developed region used for validation is defined as

$$Nu = \frac{q d_h}{k_f \left(\overline{T}_s - \overline{T}_f \right)} \qquad (28)$$
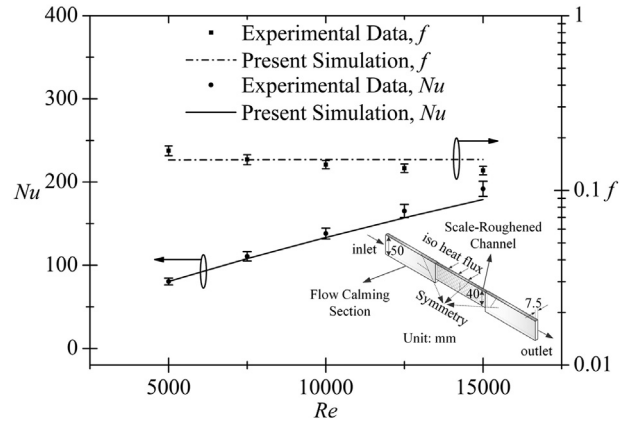
The friction factor for validation is defined as

Fig. 5. Validation of the present CFD simulation by comparing with experimental data by Chang et al. [14].

$$f = \frac{\Delta p}{\frac{1}{2} \rho u_m^2} \frac{d_h}{4L} \qquad (29)$$

4.2. Validation and verification

To verify the computational model and the method adopted in numerical simulation, preliminary computations were first conducted for a circular scale-roughened channel which had the same dimensions as the one experimentally tested by Chang et al. [14]. A quarter of the full test section is selected to be the computational domain, see Fig. 5. The readers could refer to Ref. [14] for details as to how the measurements of f and Nu were performed. From the
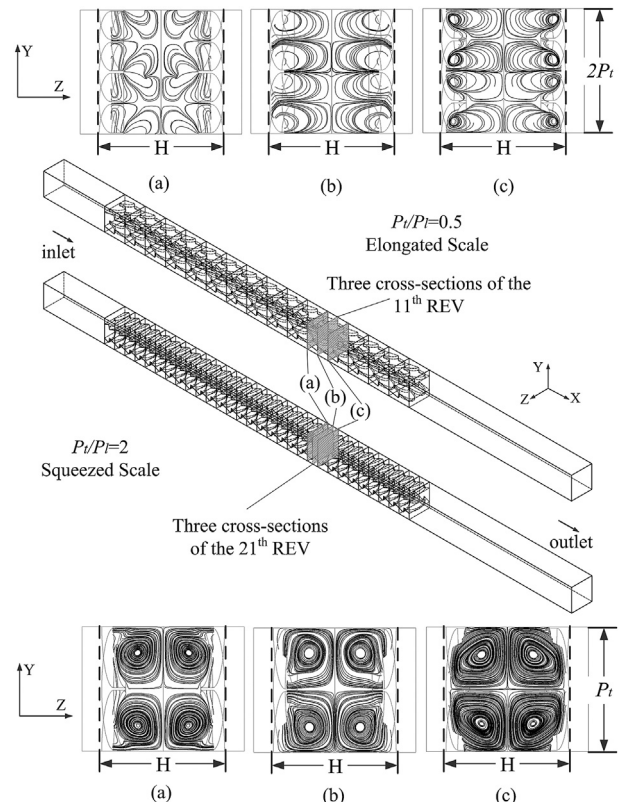

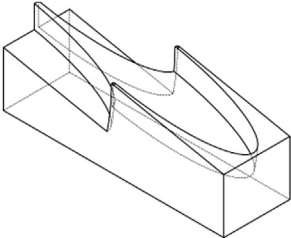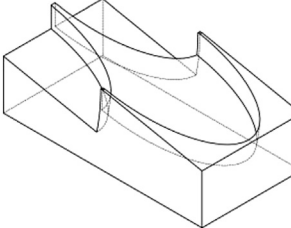**Fig. 6.** Streamlines on the planes normal to flow direction, $Re = 10000$.
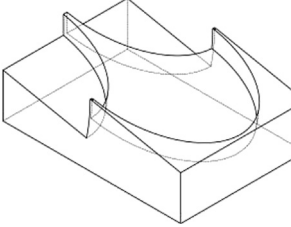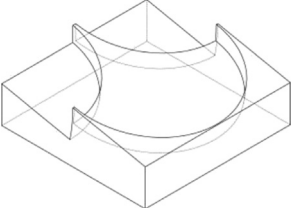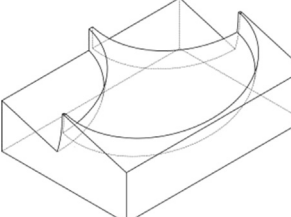
figure we can see that the maximum deviation of the Nusselt number and the friction factor from experiment are 6.3% and 12.1% with the average deviation being around 3.5% and 5.8% respectively. Our predicted results and the experimental data agree very well, thereby showing the reliability of the physical model and the adopted numerical method.

4.3. Mechanism of heat transfer enhancement by scales

To have a qualitative view into the flow behavior, Fig. 6 provides insight into the local distributions of the streamlines on three cross-sections in the y–z planes normal to the flow direction at $Re = 10,000$ for elongated scale-roughened ($P_t/P_l = 0.5$) and squeezed scale-roughened ($P_t/P_l = 2$) channels, respectively. The three planes are located at the inlet, the center plane and outlet of
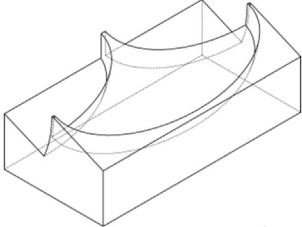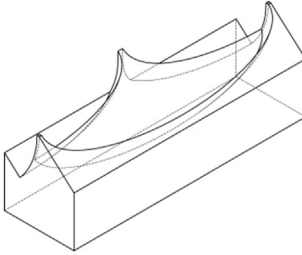
the 11th and 21st REV for elongated scale and squeezed scale respectively, showing how the streamlines develop when the fluid flows through one cycle of the elliptic scale-roughened channels. For elongated scale case, it is found that when the flow starts entering the REV, some cone-shaped streamlines are formed above the scales. After that the flow starts spinning in the spanwise direction. As the fluid flows farther downward, the spinning becomes stronger. Different from the elongated scale case, no cone-shaped streamlines are seen for the squeezed scale-roughened channel. Instead, more intense rotation is found all the way from the leading edge to the trailing edge of the scale. The strong spinning of the flow breaks the near wall boundary layers continuously and enhances the bulk flow mixing. It is easy for the readers to turn the plane streamlines into 3D footage in mind and imagine how the flow is marching in a spiral pattern. This explains why the heat

Table 2
Dimensions of the numerically tested models.

Tested models Flow direction	Scale shape	P_t/P_l	e/P_l	H/P_l
Elongated Scale, Type 1, Model 1–16		0.3	0.1, 0.15, 0.2, 0.25	0.75, 1.25, 1.75, 2.25
Elongated Scale, Type 2, Model 17–32		0.5	0.1, 0.15, 0.2, 0.25	0.75, 1.25, 1.75, 2.25
Elongated Scale, Type 3, Model 33–48		0.7	0.1, 0.15, 0.2, 0.25	0.75, 1.25, 1.75, 2.25
Circular Scale, Model 49–64		**1**	**0.1, 0.15, 0.2, 0.25**	**0.75, 1.25, 1.75, 2.25**
Squeezed Scale, Type 1, Model 65–80		1.43	0.14, 0.21, 0.29, 0.36	1.1, 1.8, 2.5, 3.2

Table 2 (*continued*)

Tested models ＼ Flow direction	Scale shape	P_t/P_l	e/P_l	H/P_l
Squeezed Scale, Type 2, Model 81–96		2	0.2, 0.3, 0.4, 0.5	1.5, 2.5, 3.5, 4.5
Squeezed Scale, Type 3, Model 97–112		3.33	0.33, 0.5, 0.67, 0.83	2.5, 4.2, 5.8, 7.5

transfer is augmented by the elliptic scale-roughened surface and why squeezed scale-roughened channels have better heat transfer performance than elongated scale-roughened channels.

4.4. Closure

Travkin and Catton [28] rigorously derive the closure terms for VAT based model from the lower scale governing equations. The closure term in the VAT momentum equation, f^*, has the form

The closure terms in the VAT energy equation, h^*, can be defined in various ways and in general will depend on how many of the integrals appearing in the VAT equation one uses and lumps into a single transport coefficient, see Travkin and Catton [28]. The nature of the equation shows that the energy transferred from the surface is integrated over an area and then divided by the chosen REV volume; therefore, the heat transfer coefficient is defined in terms of porous media morphology, usually described by specific surface and porosity.

$$f^* = 2\frac{\int_{\partial S_w} \overline{p}\cdot\mathrm{d}\vec{s}}{\rho_f A_{wp}\widetilde{\overline{u}}^2}\left(\frac{S_{wp}}{S_w}\right) + 2\frac{\int_{\partial S_w} \tau_{wL}\cdot\mathrm{d}\vec{s}}{\rho_f A_w\widetilde{\overline{u}}^2} + 2\frac{\int_{\partial S_w} \tau_{wT}\cdot\mathrm{d}\vec{s}}{\rho_f A_w\widetilde{\overline{u}}^2} - \frac{\frac{\partial}{\partial x_j}\left\langle \widehat{\overline{u}}_i\widehat{\overline{u}}_j\right\rangle_f}{\frac{1}{2}\rho_f\widetilde{\overline{u}}^2} + \frac{\frac{\partial}{\partial x_j}\left(\tilde{\nu}_T\left\langle\frac{\partial\widetilde{\overline{u}}_i}{\partial x_j}\right\rangle_f\right)}{\frac{1}{2}\rho_f\widetilde{\overline{u}}^2} \tag{30}$$

The first three terms are form drag, and laminar and turbulent contributions to skin friction, respectively. The fourth term repre-

The complete form of the closure term h^* is

$$h^* = \frac{\frac{1}{\Delta\Omega}\int_{\partial S_w}\left(k_f + k_t\right)\nabla\overline{T}_f\cdot\mathrm{d}\vec{s}}{S_w\left(\tilde{T}_s - \widetilde{\overline{T}}_f\right)} - \frac{\rho_f c_{pf}\nabla\bullet\left(\langle m\rangle\widehat{u}_f\widehat{T}_f\right)}{S_w\left(\tilde{T}_s - \widetilde{\overline{T}}_f\right)} + \frac{\nabla\bullet\left(\frac{k_f}{\Delta\Omega}\int_{\partial S_w}\overline{T}_f\mathrm{d}\vec{s}\right)}{S_w\left(\tilde{T}_s - \widetilde{\overline{T}}_f\right)} \tag{31}$$

sents the spatial flow oscillations, which are a function of porous media morphology and tell one how flow deviates from some mean value over the REV. The fifth term represents flow oscillations that are due to Reynolds stresses and are a function of porous media morphology and its time averaged flow oscillations.

In most engineered devices, the geometry is regular and a well-chosen REV will lead to only the first term being needed. The second term is identically zero for regular repeating geometries and the third is Biot number dependent. However, when in doubt, one should use the complete form given by Eq. (31).
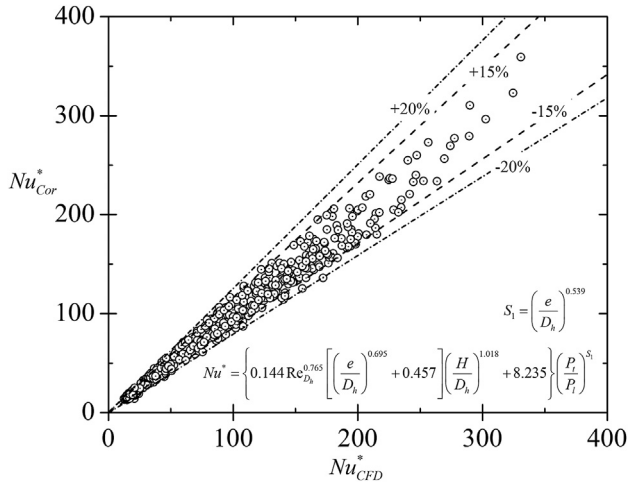
Fig. 7. Deviation of the proposed Nusselt number correlation.

Fig. 9. Comparison of the present Nusselt number correlation and rescaled experimental data, and some well-known correlations for smooth channel.

After solving the three-dimensional governing Eqs. (8), (9) and (10) with appropriate boundary conditions, the closure for the VAT based momentum equation and energy equation is obtained by integrating Eqs. (30) and (31) over the selected REV to compute the friction factor and heat transfer coefficient.

To make the correlations applicable to relatively wide range of dimensions of scale roughened channels, 112 different sets of design dimensions, see Table 2, were simulated at different Reynolds numbers, ranging from 3×10^2 to 8×10^4. The scale pitch ratio, P_t/P_l, and the ratio of the scale height to the scale longitudinal pitch, e/P_l, or the angle of attack, $\alpha = \arcsin(e/P_l)$, define the shape of the scales. The ratio of the channel height to the scale longitudinal pitch, H/P_l, specifies the shape of the channel. Therefore, P_t/P_l, e/P_l and H/P_l could specify the shape of the REV. The REVs, which have the same P_t/P_l, e/P_l and H/P_l but different scale longitudinal pitch, are dynamically similar, and they are governed by the same physical laws and associated equations, which produce exactly the same solution in terms of dimensionless variables, such as Nu and f, at the same Re. Therefore, P_t/P_l, e/P_l and H/P_l are selected to be the design parameters. However, since D_h is a function of P_t, P_l, e and H, and D_h is the chosen length scale, the heat transfer and friction closure relationships were correlated in terms of e/D_h, H/D_h, etc., using a multiple regression technique.
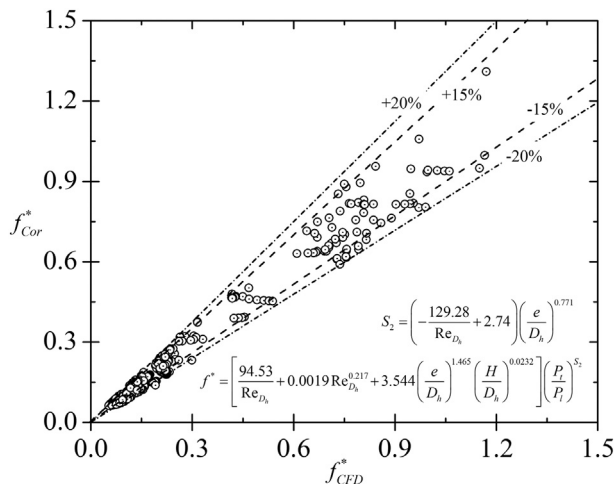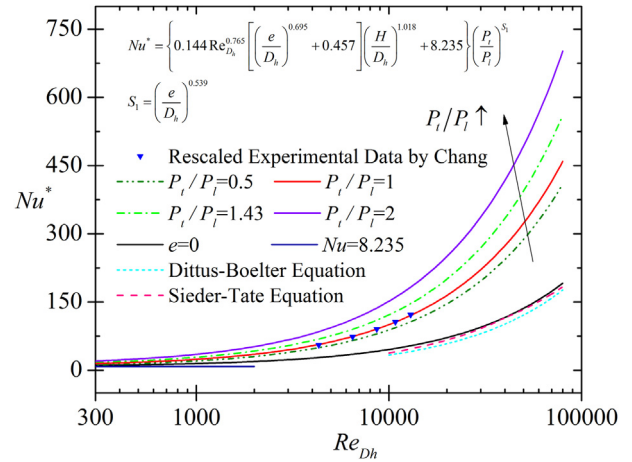
The resulting Nusselt number correlation is

$$Nu^* = \frac{h^* D_h}{\lambda_f} = \left\{ 0.144 Re_{D_h}^{0.765} \left[\left(\frac{e}{D_h} \right)^{0.695} + 0.457 \right] \left(\frac{H}{D_h} \right)^{1.018} \right.$$
$$\left. + 8.235 \right\} \left(\frac{P_t}{P_l} \right)^{S_1}$$

$$S_1 = \left(\frac{e}{D_h} \right)^{0.539}$$

(32)

The resulting friction factor is in the form

$$f^* = \left[\frac{94.53}{Re_{D_h}} + 0.0019 Re_{D_h}^{0.217} + 3.544 \left(\frac{e}{D_h} \right)^{1.465} \left(\frac{H}{D_h} \right)^{0.0232} \right] \left(\frac{P_t}{P_l} \right)^{S_2}$$

$$S_2 = \left(-\frac{129.28}{Re_{D_h}} + 2.74 \right) \left(\frac{e}{D_h} \right)^{0.771}$$

(33)

Figs. 7 and 8 show the comparison between the numerical simulation results and the results predicted by the proposed correlations. The proposed heat transfer correlation, Eq. (32), can
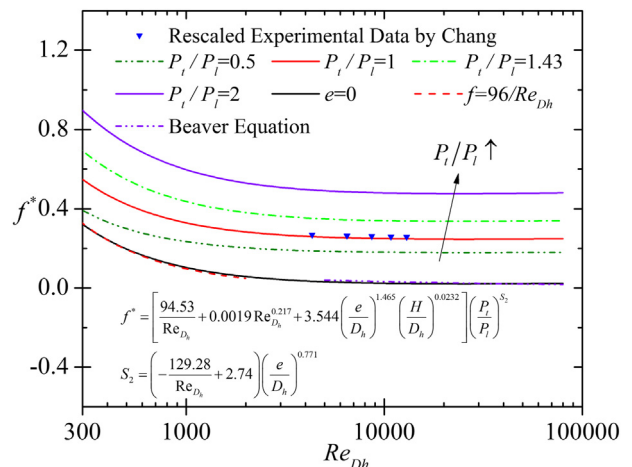

Fig. 8. Deviation of the proposed friction factor correlation.

Fig. 10. Comparison of the present friction factor correlation and rescaled experimental data, and some well-known correlations for smooth channel.

describe all the simulation results within a deviation of 20% and 91% of them within 15%. The correlation of friction factor, Eq. (33), also can predict all of them within a deviation of 20%. The correlations of Nusselt number and friction factor have an average deviation of 7.5% and 10%, respectively.

It should be noted that the present correlations are not only applicable to elliptic scale-roughened channels but also converge to those for smooth channels when $e = 0$. From the definition of D_h, Eq. (24), it is known that $D_h = 2H$ as e becomes zero and the proposed correlations converge to

$$Nu^* = 0.0325Re_{D_h}^{0.765} + 8.235 \tag{34}$$

and

$$f^* = \frac{94.53}{Re_{D_h}} + 0.0019Re_{D_h}^{0.217} \tag{35}$$

Besides, Eqs. (32) and (33) are reduced to the correlations for circular scale-roughened channels developed by Zhou et al. [19] if $P_t = P_l$. To validate the predictive capability of the present correlations, the results predicted by Eqs. (32) and (33) for different P_t/P_l with scale height of 2 mm are compared with the rescaled experimental data by Chang et al. [14] as shown in Figs. 9 and 10, see Zhou et al. [45] on how to rescale available experimental data using the VAT suggested length scale. Both Figs. 9 and 10 show that the rescaled experimental data by Chang et al. [14] and the proposed correlations agree very well.

To further check whether our correlations converged to smooth channel when $e = 0$, a few well-known correlations for smooth channels are brought into the comparison. It is shown in Fig. 9 that the converged Nu correlation, Eq. (34), for smooth parallel plate channel can predict the Nusselt number with an average deviation of 4.0% from the correlation proposed by Sieder and Tate [46] and around 12% above Dittus–Boelter equation [47] for turbulent flow. Also, when Reynolds is decreased, the Nusselt number converges to the analytical solution for laminar flow through parallel plate ducts with uniform heat flux at two walls, which is $Nu = 8.235$. From Fig. 10, it is seen that the converged friction factor correlation, Eq. (35), almost coincides with the analytical solution for laminar flow through parallel plate ducts, which is $f = 96/ReD_h$, and the correlation by Beavers et al. [48] for turbulent flow.

It should be noted that the correlations proposed in the present work are not necessarily the most accurate, however, they have wide application, are easy to use, and are quite satisfactory for most design calculations [24]. Also, for optimization, extreme accuracy is not vital because variation in the parameter being optimized can be as much as an order of magnitude.

5. Concluding remarks

Volume Averaging Theory is little more than a judicious application of Green's and Stokes' theorems to carry out the integration needed to average the point-wise conservation equations in a rigorous way. By treating the closure part of the problem carefully, the result remains rigorous in spite of its simplicity. Many everyday-engineered devices are hierarchical and heterogeneous and can be effectively treated by application of VAT. It is an approach that can be applied to many different types of transport phenomena, see Travkin and Catton [28].

The present paper describes an effort to develop a VAT based hierarchical model for a plane fin heat sink with elliptic scale-roughened surfaces and obtain the closure for the model by CFD code. The rigorously derived closure terms represented as heat transfer coefficient and friction factor were evaluated over the carefully selected REV. Correlations of friction factor and Nusselt number were established based on the simulation results.

With closure in terms of the friction factor and the heat transfer coefficient, the problem is closed and the porous media governing equations derived from VAT are functions only of porous media morphology, represented by porosity and specific surface area, and its closure. With the closure correlations, the governing equation set is relatively simple and can be solved discretely in seconds. With the help of a statistical tool for Design of Experiments (DOE) or Genetic Algorithm (GA), an elliptic scale-roughened PFHS could be designed and optimized in an hour, instead of days of CFD or experimental work. How to design and optimize an elliptic scale-roughened PFHS based on VAT will be presented in a future paper.

Nomenclature

A_w	wetted surface, m^2
A_{wp}	the cross flow projected area, m^2
c_p	specific heat, J/(kg K)
D	diameter of the scale, m
D_h	hydraulic diameter, m
d_h	hydraulic diameter defined by Chang et al. [14], m
d_p	diameter of the spherical particles, m
e	scale height, m
F_1, F_2	blending function
F_p	fin pitch, m
f	friction factor
H	channel height, m
h	heat transfer coefficient, W/(m^2 K)
k	turbulence kinetic energy per unit mass, m^2/s^2
k_f	thermal conductivity of the fluid, W/(m K)
k_s	thermal conductivity of the solid, W/(m K)
k_t	turbulent heat conductivity, W/(m K)
L	length of the channel, m
$\langle m \rangle$	porosity
Nu	Nusselt number
P_k	shear production of turbulence
Pr	Prandtl number
Pr_t	turbulent Prandtl number
P_l	longitudinal scale pitch, m
P_t	transverse scale pitch, m
p	pressure, Pa
q	heat flux, W/m^2
Re	Reynolds number
S	an invariant measure of the strain rate
S_w	specific surface, 1/m
S_{wp}	the cross flow projected area per volume, 1/m
T_s	solid temperature, K
T_f	fluid temperature, K
u_m	bulk mean flow velocity, m/s
W	width of the channel, m

Greek

α	turbulence model constant or scale attack angle (°)
β, β^*	turbulence model constant

φ_1	represent any constant in the original $k-\omega$ model ($\sigma_k, \ldots$)
φ_2	represent any constant in the transformed $k-\varepsilon$ model ($\sigma_k, \ldots$)
φ	represent the corresponding constant in the SST model ($\sigma_k, \ldots$)
μ	viscosity, Pa s
μ_t	turbulent eddy viscosity, Pa s
ν	kinematic viscosity, m^2/s
ν_t	turbulent kinematic viscosity, m^2/s
ρ	density, kg/m^3
σ_ε	$k-\varepsilon$ turbulence model constant
σ_k	turbulence model constant for the k equation
σ_ω	$k-\omega$ turbulence model constant
τ_{wL}	laminar shear stress, Pa
τ_{wT}	turbulent shear stress, Pa
$\Delta\Omega$	the volume of the REV, m^3
ω	specific turbulence dissipation rate

Subscripts and superscripts

$\sim$	a value averaged over the representative volume
$-$	an average of turbulent values
$\char94$	fluctuation of a value
$\langle f \rangle_f$	means the superficial average of the function f
f	fluid phase
t, T	turbulent
s	solid phase

References

[1] P.M. Ligrani, M.M. Oliveira, T. Blaskovich, Comparison of heat transfer augmentation techniques, AIAA Journal 41 (2003) 337–362.

[2] M.E. Taslim, T. Li, D.M. Kercher, Experimental heat transfer and friction in channels roughened with angled, V-shaped, and discrete ribs on two opposite walls, J. Turbomachinery − Transactions of ASME 118 (1996) 20–28.

[3] J.C. Han, Y.M. Zhang, C.P. Lee, Augmented heat transfer in square channels with parallel, crossed, and V-shaped angled ribs, Journal of Heat Transfer 113 (1991) 590–596.

[4] X. Gao, B. Sunden, Heat transfer and pressure drop measurements in rib-roughened rectangular ducts, Experimental Thermal and Fluid Science 24 (2001) 25–34.

[5] J.S. Park, J.C. Han, Y. Huang, S. Ou, R.J. Boyle, Heat transfer performance comparisons of five different rectangular channels with parallel angled ribs, International Journal of Heat and Mass Transfer 35 (1992) 2891–2903.

[6] H.H. Cho, S.J. Wu, H.J. Kwon, Local heat/mass transfer measurements in a rectangular duct with discrete ribs, Journal of Turbomachinery 122 (2000) 579–586.

[7] K. Park, D.-H. Choi, K.-S. Lee, Optimum design of plate heat exchanger with staggered pin arrays, Numerical Heat Transfer, Part A: Applications: An International Journal of Computation and Methodology 45 (2004) 347–361.

[8] W.A. Khan, J.R. Culham, M.M. Yovanovich, The role of fin geometry in heat sink performance, Journal of Electronic Packaging 128 (2006) 324–330.

[9] F. Zhou, I. Catton, Numerical evaluation of flow and heat transfer in plate-pin fin heat sinks with various pin cross-sections, Numerical Heat Transfer, Part A: Applications: An International Journal of Computation and Methodology 60 (2011) 107–128.

[10] G.I. Mahmood, M.L. Hill, D.L. Nelson, P.M. Ligrani, H.K. Moon, B. Glezer, Local heat transfer and flow structure on and above a dimpled surface in a channel, Journal of Turbomachinery 123 (2001) 115–123.

[11] G.I. Mahmood, P.M. Ligrani, Heat transfer in a dimpled channel: combined influences of aspect ratio, temperature ratio, Reynolds number, and flow structure, International Journal of Heat and Mass Transfer 45 (2002) 2011–2020.

[12] N.K. Burgess, P.M. Ligrani, Effects of dimple depth on channel Nusselt numbers and friction factors, Journal of Heat Transfer 127 (2005) 839–847.

[13] G.I. Mahmood, M.Z. Sabbagh, P.M. Ligrani, Heat transfer in a channel with dimples and protrusions on opposite walls, Journal of Thermophysics and Heat Transfer 15 (2001) 275–283.

[14] S.W. Chang, T.-M. Liou, M.H. Lu, Heat transfer of rectangular narrow channel with two opposite scale-roughened walls, International Journal of Heat and Mass Transfer 48 (2005) 3921–3931.

[15] S.W. Chang, T.M. Liou, K.F. Chiang, G.F. Hong, Heat transfer and pressure drop in rectangular channel with compound roughness of V-shaped ribs and deepened scales, International Journal of Heat and Mass Transfer 51 (2008) 457–468.

[16] S.W. Chang, T.L. Yang, T.-M. Liou, H.G. Fang, Heat transfer in rotating scale-roughened trapezoidal duct at high rotation numbers, Applied Thermal Engineering 29 (2009) 1682–1693.

[17] S.W. Chang, T.L. Yang, T.-M. Liou, G.F. Hong, Heat transfer of rotating rectangular duct with compound scaled roughness and V-ribs at high rotation numbers, International Journal of Thermal Sciences 48 (2009) 174–187.

[18] S.W. Chang, A.W. Lees, Endwall heat transfer and pressure drop in scale-roughened pin-fin channels, International Journal of Thermal Sciences 49 (2010) 702–713.

[19] F. Zhou, G.W. DeMoulin, D.J. Geb, I. Catton, Closure for a plane fin heat sink with scale-roughened surfaces for volume averaging theory (VAT) based modeling, International Journal of Heat and Mass Transfer 55 (2012) 7677–7685.

[20] F. Zhou, I. Catton, A numerical investigation of turbulent flow and heat transfer in rectangular channels with elliptic scale-roughened walls, Journal of Heat Transfer (2013). in press.

[21] T.B. Anderson, R. Jackson, Fluid mechanical description of fluidized beds. Equations of motion, Industrial & Engineering Chemistry Fundamentals 6 (1967) 527–539.

[22] J.C. Slattery, Flow of viscoelastic fluids through porous media, AIChE Journal 13 (1967) 1066–1071.

[23] S. Whitaker, Diffusion and dispersion in porous media, AIChE Journal 13 (1967) 420–427.

[24] S. Whitaker, Forced convection heat transfer correlations for flow in pipes, past flat plates, single cylinders, single spheres, and for flow in packed beds and tube bundles, AIChE Journal 18 (1972) 361–371.

[25] V. Travkin, I. Catton, A two-temperature model for turbulent flow and heat transfer in a porous layer, Journal of Fluids Engineering 117 (1995) 181–188.

[26] V.S. Travkin, I. Catton, Porous media transport descriptions − non-local, linear and non-linear against effective thermal/fluid properties, Advances in Colloid and Interface Science 76–77 (1998) 389–443.

[27] V.S. Travkin, I. Catton, Turbulent flow and heat transfer modeling in a flat channel with regular highly rough walls, International Journal of Fluid Mechanics Research 26 (1999) 159–199.

[28] V.S. Travkin, I. Catton, Transport phenomena in heterogeneous media based on volume averaging theory, Advances in Heat Transfer 34 (2001) 1–144.

[29] T. Masuoka, Y. Takatsu, Turbulence model for flow through porous media, International Journal of Heat and Mass Transfer 39 (1996) 2803–2809.

[30] B.V. Antohe, J.L. Lage, A general two-equation macroscopic turbulence model for incompressible flow in porous media, International Journal of Heat and Mass Transfer 40 (1997) 3013–3024.

[31] A. Nakayama, F. Kuwahara, A macroscopic turbulence model for flow in a porous medium, Journal of Fluids Engineering 121 (1999) 427–433.

[32] M.H.J. Pedras, M.J.S. de Lemos, Macroscopic turbulence modeling for incompressible flow through undeformable porous media, International Journal of Heat and Mass Transfer 44 (2001) 1081–1093.

[33] A. Horvat, I. Catton, Numerical technique for modeling conjugate heat transfer in an electronic device heat sink, International Journal of Heat and Mass Transfer 46 (2003) 2155–2168.

[34] A. Horvat, I. Catton, Application of Galerkin method to conjugate heat transfer calculation, Numerical Heat Transfer, Part B: Fundamentals: An International Journal of Computation and Methodology 44 (2003) 509–531.

[35] A. Horvat, B. Mavko, Hierarchic modeling of heat transfer processes in heat exchangers, International Journal of Heat and Mass Transfer 48 (2005) 361–371.

[36] A. Horvat, B. Mavko, Calculation of conjugate heat transfer problem with volumetric heat generation using the Galerkin method, Applied Mathematical Modelling 29 (2005) 477–495.

[37] A. Vadnjal, Modeling of a Heat Sink and High Heat Flux Vapor Chamber. PhD thesis, in: Aerospace Engineering, University of California Los Angeles, Los Angeles, 2009, p. 209.

[38] F. Zhou, I. Catton, Volume averaging theory (VAT) based modeling and closure evaluation for fin-and-tube heat exchangers, Heat and Mass Transfer 48 (2012) 1813–1823.

[39] K. Vafai, Handbook of Porous Media, Marcel Dekker, Inc., New York, 2000.

[40] K. Vafai, Handbook of Porous Media, Taylor & Francis, 2005.

[41] S. Whitaker, The Method of Volume Averaging, Kluwer Academic Publishers, Boston, 1999.

[42] F. Zhou, N.E. Hansen, D.J. Geb, I. Catton, Determination of the number of tube rows to obtain closure for volume averaging theory based model of fin-and-tube heat exchangers, Journal of Heat Transfer 133 (2011) 121801.

[43] F.R. Menter, Two-equation eddy-viscosity turbulence models for engineering applications, AIAA Journal 32 (1994) 1598–1605.

[44] F.R. Menter, M. Kuntz, R. Langtry, Ten years of industrial experience with the SST turbulence model, Turbulence, Heat and Mass Transfer 4 (2003) 625–632.

[45] F. Zhou, N.E. Hansen, D.J. Geb, I. Catton, Obtaining closure for fin-and-tube heat exchanger modeling based on volume averaging theory (VAT), Journal of Heat Transfer 133 (2011) 111802.

[46] E.N. Sieder, G.E. Tate, Heat transfer and pressure drop of liquids in tubes, Industrial & Engineering Chemistry 28 (1936) 1429–1435.

[47] K.E. Gungor, R.H.S. Winterton, A general correlation for flow boiling in tubes and annuli, International Journal of Heat and Mass Transfer 29 (1986) 351–358.

[48] G.S. Beavers, E.M. Sparrow, J.R. Lloyd, Low Reynolds number turbulent flow in large aspect ratio rectangular ducts, Transactions of ASME, Series D, Journal of Basic Engineering 93 (1971) 296–299299.